Observation of Hydronium Ions at the Air−Aqueous Acid Interface: Vibrational Spectroscopic Studies of Aqueous HCl, HBr, and HI

Lori M. Levering, M. Roxana Sierra-Hernández, and Heather C. Allen*

Department of Chemistry, The Ohio State University, 100 W. 18th Ave., Columbus, Ohio 43210

Received: September 1, 2006; In Final Form: December 28, 2006

The air−liquid interface of aqueous hydrogen-halide solutions is examined using vibrational sum frequency generation spectroscopy. Infrared and Raman spectroscopies are used to compare the effects of the ions on the water structure in the bulk solutions to that of the interface. The addition of HCl, HBr, and HI to water is found to cause a significant disruption in the hydrogen-bonding network at the air−liquid interface, similar to that which is observed for sodium halides. However, a convolution of additional effects are observed for acids at the air−aqueous interface: interfacial H_3O^+ (and $H_5O_2^+$) which gives rise to surface potential changes, an increase in interfacial depth from interfacial concentration gradients, and a decrease in the number of dangling OH bonds relative to the neat water surface. Additionally, and moreover, sum frequency spectra reveal a surface proton continuum at frequencies below 3000 cm^{-1}, indicating that hydronium ions (and Zundel ions) exist at the air−aqueous interface.

I. Introduction

In the past decade, atmospheric aerosol surface chemistry has been recognized to play a critical role in the uptake and transformation of gaseous species present in the atmosphere.[1−3] Although it is acknowledged that heterogeneous reactions of aerosols impact the atmosphere, fundamental questions still remain concerning surface species and reaction mechanisms. In addition, the identity and orientation of the species at the surface of these aerosols impact the physical characteristics of the surface (e.g., hydrophobicity) and thus influence the initial adsorption of gas-phase molecules.

The ubiquitous nature of water in atmospheric aerosols makes investigating the air−aqueous interface a natural first step in understanding both the physical and chemical processes of aerosols. A molecular level understanding of the air−aqueous acid interface is gained by examining the effects of halide ions and protons on the surface structure of water. Fundamental studies can then provide insight into the role of acidic species at the surface of atmospheric aerosols and atmospheric heterogeneous reaction mechanisms.[1,3] In light of this, investigations into the bulk and interfacial structure of hydrogen halide (i.e., strong acid) solutions are presented. Vibrational sum frequency generation (VSFG) spectroscopy is used to examine the air−liquid interface of hydrogen halide aqueous solutions, providing detailed, microscopic information about the distribution of ions at the air−water interface. Surface tension measurements are also used to gain a macroscopic view of the air−aqueous interface. In order to draw a comparison between the interface and the bulk solution, the hydrogen halide aqueous solutions are investigated with Raman and infrared spectroscopies. Therefore, the theoretical relationship between the SFG, Raman, and IR is elucidated in the Experimental Section.

* To whom correspondence should be addressed. E-mail: allen@chemistry.ohio-state.edu.

II. Experimental Section

A. Sum Frequency Generation Background. Since the focus of this work is on the surfaces of aqueous solutions, a brief overview of VSFG theory is presented. A more in depth discussion of the theory of VSFG and SFG can be found in the literature.[4−11]

VSFG is a second-order nonlinear process in which two pulsed laser beams, one with infrared frequency, ω_{IR}, and one with visible frequency, ω_{Vis}, are overlapped in a medium in time and space, generating a photon at the sum of the frequencies, $\omega_{SFG} = \omega_{IR} + \omega_{Vis}$. Under the electric dipole approximation, the SFG process only occurs in noncentrosymmetric environments, such as an interface. It is important to note that a surface is by definition SFG-active. However, if lack of inversion symmetry extends below the surface layer, then this region is also SFG-active. In SFG work, the noncentrosymmetric surface region is then defined as the "interface". The interfacial region can extend many layers beyond the surface region. We tend to use the words interface and surface interchangeably in the SFG literature, with the assumption that the SFG-active region defines what we call the surface (or interface). Yet, the term "interface" is more technically correct for SFG studies.

The SFG intensity, I_{SFG}, is proportional to the square of the surface nonlinear susceptibility, $\chi^{(2)}$, which is a function of the sum frequency ($\omega_{SFG} = \omega_{IR} + \omega_{Vis}$) generated from noncentrosymmetric media.

$$I_{SFG} \propto |P_{SFG}|^2 \propto |\chi^{(2)}_{NR} + \sum_{\nu} |\chi^{(2)}_{\nu}| e^{i\delta_\nu}|^2 I_{IR} I_{vis} \qquad (1)$$

P_{SFG} is the sum frequency nonlinear second-order polarization. $\chi^{(2)}_{NR}$and $\chi^{(2)}_{\nu}$ are the nonresonant and resonant parts of $\chi^{(2)}$, respectively. δ_ν is the phase factor, and I_{IR} and I_{vis} are the intensities of the incident infrared and visible beams. (The Fresnel terms, which essentially act to reduce the SFG intensity

10.1021/jp065694y CCC: $37.00
Published on Web 02/22/2007

and are angle and polarization dependent,[11] have been omitted.) When the frequency of the incident infrared beam is resonant with a vibrational mode, ν, of an interfacial molecule, the resonant susceptibility term, $\chi_\nu^{(2)}$, dominates and an SFG intensity enhancement is observed (the nonresonant term $\chi_{NR}^{(2)}$ is relatively small, but not negligible).

Different polarization combinations of the incident and outgoing fields can be used to provide orientational[12] and vibrational mode information about the molecules within the interface. Liquid surfaces and interfaces are isotropic in the plane of the surface (i.e., the surface has $C_{\infty v}$ symmetry), and thus, symmetry considerations[5] can reduce the surface susceptibility $\chi_s^{(2)}$, a 27-element tensor, to four independent nonzero elements

$$\chi_{zzz}^{(2)};\ \chi_{xxz}^{(2)}=\chi_{yyz}^{(2)};\ \chi_{xzx}^{(2)}=\chi_{yzy}^{(2)};\ \chi_{zxx}^{(2)}=\chi_{zyy}^{(2)} \tag{2}$$

where z is the direction normal to the interface.

These four different elements contribute to the VSFG signal under the four different polarization conditions PPP, SSP, SPS, and PSS, where the polarizations are listed in the order of decreasing frequency (sum frequency, visible, IR). P-polarized light is defined as having its electric field vector parallel to the plane of incidence and S-polarized light has its electric field vector perpendicular to the plane of incidence. The different polarization combinations are sensitive to the direction of the IR and Raman transition moments, where the PPP polarization combination includes all components of the resonant vibrational mode.

The resonant macroscopic nonlinear susceptibility, $\chi_\nu^{(2)}$, can be further broken down as shown in eq 3

$$\chi_\nu^{(2)} \propto \frac{A_\nu}{\omega_\nu - \omega_{IR} - i\Gamma_\nu} \tag{3}$$

where A_ν is the amplitude of the transition moment, ω_ν is the resonant frequency, ω_{IR} is the frequency of the incident IR beam, and Γ_ν describes the half-width at half-maximum (hwhm) of the transition. The sign of A_ν indicates whether a transition is out of phase with respect to the other transitions or if two transition moments exist antiparallel with respect to each other; the resultant SFG response for both cases will then be 180° out of phase. A_ν includes both the Raman and the infrared contributions; therefore, SFG is allowed when the vibrational transition is both Raman and infrared active.

To further illustrate this point, the macroscopic susceptibility, $\chi_{IJK,\nu}^{(2)}$, can be calculated from the molecular susceptibility, $\beta_{IJK,\nu}$, as shown in eq 4

$$\chi_{IJK,\nu}^{(2)} = N\langle\beta_{IJK,\nu}\rangle \tag{4}$$

where $\chi_{IJK,\nu}$ is equal to the number density, N, multiplied by the orientation average of $\beta_{IJK,\nu}$, and I,J,K represents the laboratory coordinates. An Euler angle transformation relates the laboratory coordinate system (I,J,K) to the molecular coordinate system (l,m,n). The transformation is shown in eq 5

$$\beta_{IJK,\nu} = \sum_{lmn} \mu_{IJK:lmn}\beta_{lmn,\nu} \tag{5}$$

where $\mu_{IJK:lmn}$ is the Euler angle transformation between the laboratory coordinates I,J,K and the molecular coordinates l,m,n. The molecular susceptibility, $\beta_{lmn,\nu}$, can be described by eq 6

$$\beta_{lmn,\nu} = \frac{\langle g|\alpha_{lm}|\nu\rangle\langle\nu|\mu_n|g\rangle}{\omega_{IR} - \omega_\nu + i\Gamma_\nu} \tag{6}$$

where α_{lm} represents the Raman tensor for the transition moment $\langle g|\alpha_{lm}|\nu\rangle$, and $\langle\nu|\mu_n|g\rangle$ represents the IR transition moment for the molecule.

VSFG Scanning System and Experimental Details. The experimental setup of the 10 Hz scanning VSFG system has been described previously.[13] The SFG experiments (except Figure 8) were carried out using a visible beam at 532 nm and an infrared beam tunable from 2500 to 4000 cm^{-1} with a bandwidth of ~8 cm^{-1} generated from a KTP-KTA based optical parametric generator/amplifier (OPG/OPA) system (LaserVision). The 532 nm beam is generated by doubling the frequency (second harmonic) of the 1064 nm pump source from an EKSPLA PL 2143 A/SS Nd:YAG laser (29 ps pulse duration and 10 Hz repetition rate). The 532 nm beam is focused after the liquid surface using a plano-convex lens to yield a beam diameter of ~1 mm with a pulse energy of ~1.1 mJ. The IR beam is focused at the sample surface using a BaF_2 lens to yield a diameter of <0.5 mm. The peak IR energy (at 3300 cm^{-1}) was ~700 μJ. The IR profile was measured simultaneously with the SFG spectrum by reflecting ~5% of the beam intensity onto an IR energy meter (J9LP, Molectron Inc.) using a BaF_2 window. The VSFG intensity decreased corresponding to the quantitative reduction of the infrared energy as dictated by eq 1, confirming that the vibrational modes were below saturation.

The input angles were set to ~45° and ~53° from the surface normal for the 532 nm and IR beams, respectively. A 512 × 512 pixel back-illuminated charge coupled device (CCD; Andor Technology, DV887ECS-BV) cooled to −80 °C was used to detect the sum frequency signal. A series of irises, a Schott glass filter (BG25), and two holographic Notch-Plus filters (Kaiser Optical Systems, Inc., HNPF-532.0−1.0) were used to block the 532 nm scattered light.

The SFG signal was optimized spatially and temporally at 3300 cm^{-1}. The VSFG spectra (including Figure 8) were normalized by the IR profile since the IR is detected in real-time with the SFG intensity. The VSFG spectrum was also obtained from the surface of a GaAs crystal, which accounts for any anomalies in the temporal and spatial overlap, and was comparable to the IR spectrum. The polarization combinations used for the SFG experiments were S, S, and P for the SFG, 532 nm, and infrared beams, respectively. All VSFG spectra were acquired at 21 ± 2 °C.

The SSP-polarized spectra presented (except Figure 8) were acquired using a 10 s exposure time for each data point and were acquired in ~30 min (from 2800 to 3950 cm^{-1}). The VSFG spectra of the acid solutions are an average of two spectra and have been reproduced several times over the period of 2 years. At least one air−neat water spectrum was acquired at the beginning and the end of the daily experiments to ensure the stability of the SFG system and to confirm reproducibility.

The VSFG spectra shown in Figure 8 were acquired using a 20 Hz scanning VSFG system from EKSPLA. In this system, a 1064 nm EKSPLA PL 2143A/20/SS Nd:YAG laser (27 ps pulse duration and 20 Hz repetition rate) pumps an EKSPLA PG401/DFG2-16P optical parametric generator (OPG). The peak IR energy (at 2940 cm^{-1}) was 51 μJ per pulse and the 532 nm beam was 370 μJ per pulse. The input angles for the 20 Hz visible and infrared beams were 66.3° and 56.8°, respectively. A photomultiplier tube (PMT Hamamatsu, R5929) was used to detect the sum frequency signal. The SSP-polarized VSFG spectra shown in Figure 8 were acquired using a 15 s exposure time for each data point and are an average of two spectra.

B. Raman Spectroscopy. Polarized Raman spectra (isotropic and anisotropic) were collected by passing the 532 nm light from a CW laser (Spectra-Physics, Millennia II, ~82 mW) onto the sample using a fiber optic probe (InPhotonics, RPS532/12−15). The scatter was focused onto the entrance slit of a 303 mm monochromator (Andor Technology, Shamrock 303i) using a BK7 lens. The scatter was dispersed using a 600 g/mm grating blazed at 500 nm and collected on a thermoelectrically cooled CCD camera (Andor Technology, DU440-BV, 2048 × 512 pixel array, back-illuminated, cooled to −70 °C). Andor MCD software was used for data collection and display (Andor Technology, version 2.63.0.5). A 90° configuration for the incoming laser beam and detection was used and sheet polarizers were placed before and after the sample to select the polarization of the incident light and the Raman scatter, respectively. A Lyot depolarizer (Thorlabs, LDPOL) was placed in the light path before the monochromator since there is a polarization dependence for the diffraction grating. The slit width was set to 50 μm, and the bandpass was ~10 cm^{-1}. (Anisotropic and higher resolution unpolarized Raman spectra can be found in Supporting Information.) The acquisition temperature was 23 ± 1 °C. The CCD camera was calibrated using the 435.83 nm line of a fluorescence lamp; the wavenumber position was confirmed by taking a spectrum of crystalline naphthalene and comparing peak positions with the literature values.[14]

C. ATR-FTIR Spectroscopy. A Thermo Nicolet FTIR spectrometer (Avatar 370, Thermo Electron Corporation) was employed in the ATR-FTIR (attenuated total reflection Fourier transform infrared) spectroscopy experiments. ATR-FTIR was used as a bulk probe instead of transmission FTIR spectroscopy in these studies; we have assumed that the solution refractive indices are relatively constant. A 45° single bounce silicon crystal trough ATR accessory (Smart SpeculATR, Thermo Electron Corporation) was used to collect the spectra at a spectral resolution of 4 cm^{-1} at ~24 °C. The spectra were averaged over 64 scans.

D. Spectral Fits. The VSFG spectrum describes the SFG intensity (I_{SFG}) as a function of the incident infrared frequency (ω_{IR}) and can be mathematically fit according to eqs 1 and 3. When performing the fit, a constant complex number is used as the nonresonant term ($\chi^{(2)}_{NR}$) and the sign of the amplitude (A_ν) is used to denote the phase of the photons of the vibrational mode from the interfacial molecules, which incorporates orientation and relative vibrational phases. Equation 3 indicates the Lorentzian line shape in the VSFG spectrum fitting. In the VSFG fitting, initial guesses were based on the Raman and IR fits for neat water. Once the neat water VSFG spectrum was fit with allowing all parameters to vary, these values were used as initial guesses in the aqueous acid VSFG fits. In some cases, in order to isolate the additional contributions, the neat water VSFG spectral parameters were held constant or held in a range near the initial value. Otherwise, nonphysical fits were obtained in many cases. In Raman and IR fitting, the intensity is the summation of each vibration's intensity ($|A|^2 + |B|^2$), whereas in SFG, the intensity is the absolute square of the summation of each vibration's ($\chi^{(2)}_\nu$) and ($\chi^{(2)}_{NR}$) as shown in eq 1. This leads to different spectral characteristics for VSFG spectra relative to Raman and IR spectra. Therefore, VSFG spectra interpretation should occur after deconvolution into the component peaks because direct comparison of VSFG spectra to Raman and IR spectra may be misleading, particularly for the broad bands of the hydrogen-bonded stretching region (3000−3600 cm^{-1}).

E. Surface Tension. Surface tensions were measured using a surface tensiometer (DeltaPi, Kibron Inc.), which employs the Wilhelmy Plate technique. A minor modification in the technique was made in that a wire probe was used instead of a thin plate. The solutions were contained in Teflon wells for the measurements. Surface tension measurements were collected at 25.0 ± 0.5 °C and are an average of three values. Error bars are one standard deviation.

F. Chemicals. Water was obtained from a Millipore Nanopure system (18.3 MΩ·cm). Acid solutions were made volumetrically from concentrated HCl (Fisher Scientific, 36.5 wt. %), HBr (Fisher Scientific, 48 wt. %), and HI (Alfa Aesar, 47 wt. %) solutions. Sodium halide salts (certified ACS grade) were purchased from Fisher Scientific. To prevent photochemistry from occurring, the HI and NaI solutions were stored in a dark cabinet and the flasks were covered with aluminum foil. In addition, HI solutions were made no more than 1 day in advance of their use. The NaCl, NaBr, and NaI salts contained a significant amount of organic contamination, and therefore, solutions were filtered with an activated carbon filter (Whatman, CARBON-CAP 150) to remove these contaminants (except Figure 8). The NaBr salt used to acquire VSFG spectra shown in Figure 8 was baked in a muffle furnace (Fisher Isotemp) for 6 h at 650 °C to eliminate organic contaminants. All of the solutions were checked for organic contamination by obtaining VSFG spectra of the solutions in the region between 2800 and 3000 cm^{-1}.

III. Results and Discussion

The IR and Raman spectra of bulk neat water and the SSP-polarized VSFG spectrum of the air−neat water interface in the O−H stretch region (2900−3900 cm^{-1}) are shown in Figure 1, panels a−c, respectively, along with their calculated fits and component peaks (Table 1).

The broad peaks in the 3000−3600 cm^{-1} region are fit to three bands positioned at ~3250, ~3450, and ~3550 cm^{-1} in the IR, Raman, and VSFG spectra. The broadness and line shape of these O−H stretching bands indicate a range of hydrogen-bonding strengths, consistent with theory[15−18] and experiments[17,18] that have shown that the dynamics of the hydrogen-bonding network plays a dominant role in the spectral shape of liquid water in the OH stretching region. Due to recent theoretical research[17,18] showing that a continuum of hydrogen-bonding lengths can contribute to the apparent structure of the vibrational spectra for condensed phase water, we assign the 3000−3600 cm^{-1} region to this continuum. The component peak fits of this region are used to compare band areas, and therefore, number densities. The lower frequencies beginning at ~3000 cm^{-1} arise from stretching modes of strongly hydrogen bonded (SHB) water molecules within a hydrogen-bonding network.[19,20,21] As one moves to higher frequencies, the observed resonances arise from less strongly hydrogen bonded (LSHB) water molecules. The assignments of surface water O−H stretches for the air−neat water interface are based on this same premise, with the exception of the ~3250 cm^{-1} peak in the VSFG spectrum (3229 cm^{-1}). This band is primarily attributed to the bonded O−H of the 3-coordinate water molecules at the surface that are single proton donor−double proton acceptor (DAA) molecules,[20,22,23] in addition to 4-coordinate water species that are SHB. Upon adding a solute to neat water or at water-solid interfaces,[24] SHB 4-coordinate water molecules can dominate the spectral response due to interfacial width increases and, in some cases, surface potentials.

The 4-coordinate and LSHB water molecules at the surface exist as distorted tetrahedrons. The O−H stretches of these molecules are the major contribution to the higher frequencies in the VSFG spectrum.[20,22,23,25−28]

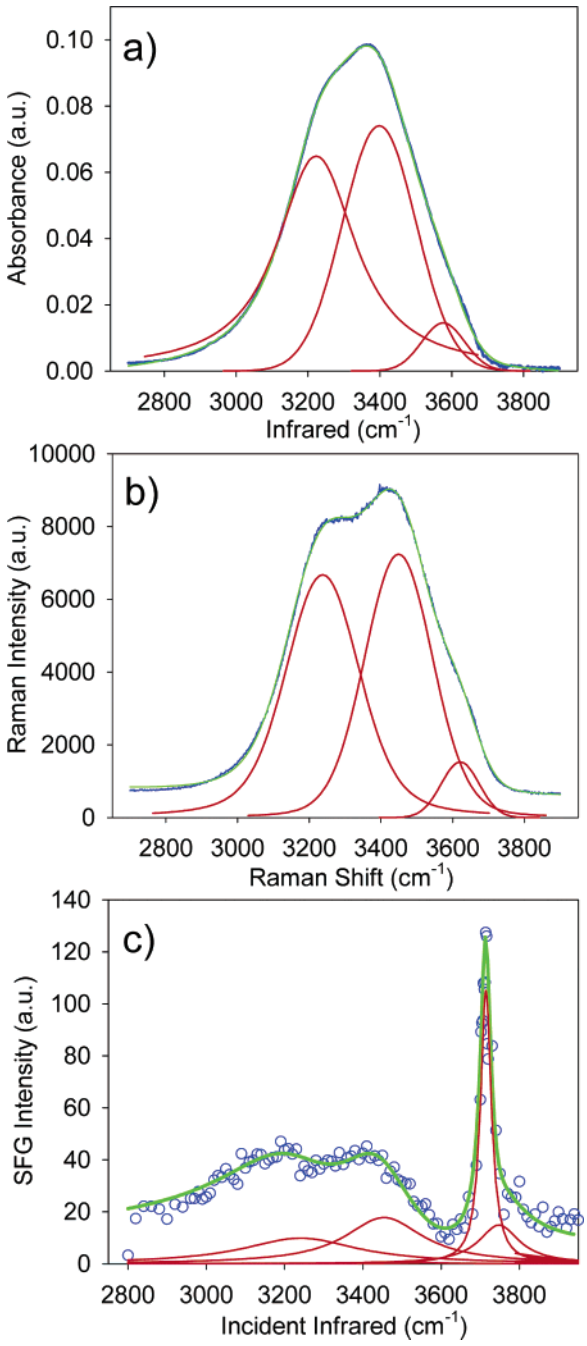

Figure 1. (a) ATR-FTIR spectrum of neat water, (b) Isotropic Raman spectrum of neat water, and (c) SSP-polarized VSFG spectrum of the air−neat water interface. The component peaks are shown in red and the calculated spectra from the spectral fits are shown in green.

Not part of the continuum in the VSFG spectrum is a relatively narrow peak at 3700 cm^{-1}, which is assigned to the dangling O−H (free O−H) stretch of water molecules bridging the air−aqueous interface with one uncoupled O−H bond directed into the vapor phase[26,30,31] and the other interacting through hydrogen bonding with the liquid phase as described above.[20,22,23,28]

VSFG intensity is also observed on the high-frequency side of the free O−H peak at 3748 cm^{-1}; however, the origin of this intensity is not well understood.[28] This intensity is minimal in the neat water VSFG spectrum (but is significantly larger in the spectra of the aqueous acids as is shown later) and is not likely derived from the continuum tail. One possible explanation is a combination band of the OH stretch with a hindered rotation of water molecules at the surface.[32] Another possible explanation for the intensity of the high-frequency side of the free O−H is surface water distortion, perhaps due to the less than optimal tetrahedral hydrogen-bonding substructure as described in cluster studies.[33] This assignment is supported by aqueous ammonia studies by Shultz and co-workers[28] which suggests that the free O−H consists of two components. Additionally, recent work by Shin et al.[34] supports the existence of two peaks at ∼3700 and ∼3720 cm^{-1} in water clusters. The low-frequency peak is assigned to the free O−H stretch of DAA water molecules as stated above and the high-frequency peak is assigned to two-coordinate DA water molecules. There is also evidence from IR spectroscopic studies on amorphous ice surfaces supporting the assignment to the dangling O−H from doubly coordinated water molecules.[19,35,36] Thus, a component peak on the high-frequency side of the free O−H is used to fit the IR-normalized VSFG spectra since a nonresonant component did not compensate for the resonant-like feature, particularly in the HI spectra as well as in previous SFG spectra of sodium halide solution surfaces.[13,28]

To understand the bulk hydrogen-bonding environment of water after addition of strong acids, a series of Raman and ATR-FTIR spectra were obtained for 0.015*x*, 0.050*x*, and 0.10*x* hydrochloric (HCl), hydrobromic (HBr), and hydriodic (HI) acids (x = mole fraction). The ATR-FTIR spectra are shown in Figure 2, and the isotropic Raman spectra (polarized parallel to the electric field vector of the incident vertically polarized laser beam) are shown in Figure 3. Peak positions, amplitudes, full width at half-maximum (fwhm), and peak areas for the IR and Raman spectra are shown in Table 1. The fitting of the ATR-FTIR and Raman spectra of the acids is complicated by the presence of the proton hydration complexes, H_3O^+ and $H_5O_2^+$.[37−40] These complexes have a broad absorption in the IR spectra and to a lesser extent in the Raman spectra. Therefore, an additional broad and low-intensity band had to be included when fitting the acid spectra.

With the addition of acid (HCl, HBr, and HI) to water, the IR spectra show a decrease in the 3250 cm^{-1} peak and a decrease and narrowing of the 3450 cm^{-1} peak. The IR spectra of the acids also reveal a substantial intensity enhancement in the region between ∼1500 and ∼3200 cm^{-1}. The Raman spectra of the acids show a decrease in the 3250 cm^{-1} peak accompanied by an increase and narrowing of the 3450 cm^{-1} peak. The broad band observed in the IR spectra from ∼1500 and ∼3200 cm^{-1} is also present in the Raman spectra but to a lesser extent. These changes in the IR and Raman spectra are amplified when going from 0.015*x* to 0.10*x*, as well as when the size and polarizability of the anion is increased ($Cl^- < Br^- < I^-$).

The changes in the hydrogen-bonded stretching region of the IR and isotropic Raman spectra upon the addition of HCl, HBr, and HI relative to that of neat water is attributed to the water molecules breaking their symmetric hydrogen-bonding network to solvate the ions. The addition of ions to water disrupts the symmetric stretch character of the tetrahedral hydrogen-bonding network, and thus a decrease in the 3250 cm^{-1} peak intensity. The resulting increase in LSHB water molecules is observed in the increase of the 3450 cm^{-1} peak intensity of the Raman spectra. (For 6.1 M aqueous sodium bromide solutions (Supporting Information), the IR spectra reveal an increase in the 3450 cm^{-1} peak.) The trend in the 3450 cm^{-1} peak in the acid solutions is associated with an increase in the size and polarizability of the anion in solution ($Cl^- < Br^- < I^-$) as well as an increase in concentration. As the acid concentration is increased, an ever-increasing fraction of the water molecules

TABLE 1: Parameters for ATR-FTIR and Isotropic Raman Spectral Fits of HCl, HBr, and HI Concentration Series

	ATR-FTIR				Raman			
	peak position (cm^{-1})	amplitude (A_v)	fwhm ($2\cdot\Gamma_v$)	area	peak position (cm^{-1})	amplitude (A_v)	fwhm ($2\cdot\Gamma_v$)	area
neat water	3226	0.0923	259	27.4	3241	4479	232	1.22×10^6
	3401	0.0761	233	18.9	3445	4807	208	1.18×10^6
	3576	0.0163	146	2.5	3612	1037	127	1.55×10^5
0.015*x* HCl	2755	0.0035	791	2.9	3083	601	324	2.07×10^5
	3224	0.0958	277	29.2	3239	3603	198	7.59×10^5
	3401	0.0747	236	18.7	3444	5253	219	1.23×10^6
	3575	0.0149	140	2.2	3622	927	132	1.30×10^5
0.015*x* HBr	2733	0.0037	866	3.4	3075	605	266	1.71×10^5
	3225	0.0960	277	29.1	3232	3609	187	7.19×10^5
	3404	0.0745	232	18.4	3440	5448	234	1.35×10^6
	3574	0.0152	140	2.3	3626	837	126	1.12×10^5
0.015*x* HI	2610	0.0033	891	3.1	3106	605	370	2.38×10^5
	3223	0.1018	280	29.1	3235	3262	194	6.74×10^5
	3405	0.0741	237	18.7	3450	5432	233	1.35×10^6
	357	0.0148	140	2.2	3627	692	122	8.99×10^5
0.050*x* HCl	2816	0.0114	770	9.4	3004	602	327	2.23×10^5
	3222	0.0955	306	30.3	3242	3087	217	7.13×10^5
	3402	0.0672	230	16.5	3452	5513	218	1.28×10^6
	3570	0.0141	138	2.1	3626	598	118	7.50×10^5
0.050*x* HBr	2815	0.0110	774	9.1	3089	601	410	2.62×10^5
	3221	0.0952	303	28.6	3240	2976	202	6.38×10^5
	3407	0.0701	230	17.2	3454	5665	224	1.35×10^6
	3571	0.0140	135	2.0	3630	597	119	7.57×10^5
0.050*x* HI	2806	0.0095	769	7.8	3090	589	447	2.81×10^5
	3222	0.1032	302	27.9	3243	2800	208	6.21×10^5
	3414	0.0697	231	17.1	3464	6400	222	1.51×10^6
	3569	0.0144	136	2.1	3631	407	109	4.74×10^5
0.10*x* HCl	2821	0.0215	764	17.5	2939	658	561	4.02×10^5
	3213	0.0749	329	27.0	3252	2797	233	7.84×10^5
	3399	0.0601	240	15.4	3452	5259	210	1.19×10^6
	3566	0.0111	132	1.6	3624	400	119	5.01×10^5
0.10*x* HBr	2820	0.0195	767	15.9	3093	696	541	4.01×10^5
	3214	0.0755	325	25.8	3242	2525	208	5.60×10^5
	3405	0.0661	233	16.4	3457	6370	220	1.49×10^6
	3566	0.0125	131	1.8	3636	370	105	4.12×10^5
0.10*x* HI	2818	0.0165	762	13.4	3108	696	543	4.02×10^5
	3217	0.0781	320	24.8	3254	2236	215	5.11×10^5
	3416	0.0678	228	16.5	3465	7296	207	1.60×10^6
	3565	0.0139	131	1.9	3628	371	115	4.54×10^5

becomes associated with the hydration shells of the anions. The resulting effect is an increasing perturbation of the hydrogen-bonding network and thus is observed as an increase in the 3450 cm^{-1} peak. These results are consistent with previous studies of aqueous acid[37] and sodium halide solutions.[13]

The Raman spectra clearly reveal a higher sensitivity to the ion solvation effects. In Figure 4, the unpolarized Raman spectra of 0.10*x* HCl, NaCl, HBr, and NaBr are shown and reveal the differences between the aqueous acid and salt solutions. (The unpolarized and isotropic Raman spectra show the same trends, as one would expect for this chemical system.) The sodium cations contribute to the rise in the 3450 cm^{-1} peak, thus enhancing the intensity; this is in contrast to the lack of contribution provided by the hydrated proton in the 3450 cm^{-1} region. Yet, there are subtle changes in the shape of the Raman spectra arising from the hydrated proton, which includes an enhancement in intensity on the lower energy side of the hydrogen-bonded stretching region of water.

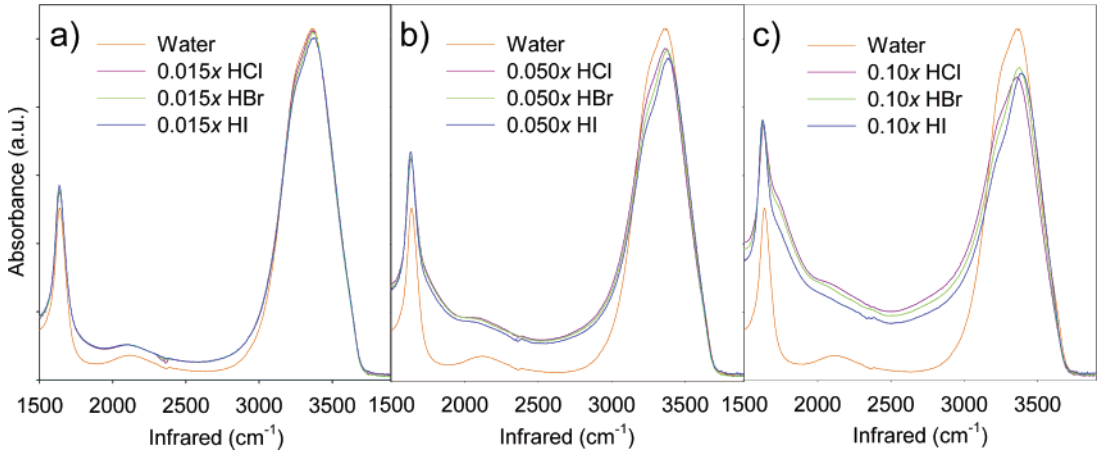

Figure 2. ATR-FTIR spectra of HCl, HBr, and HI aqueous solutions compared to that of neat water (a) 0.015*x*, (b) 0.050*x*, and (c) 0.10*x* series.

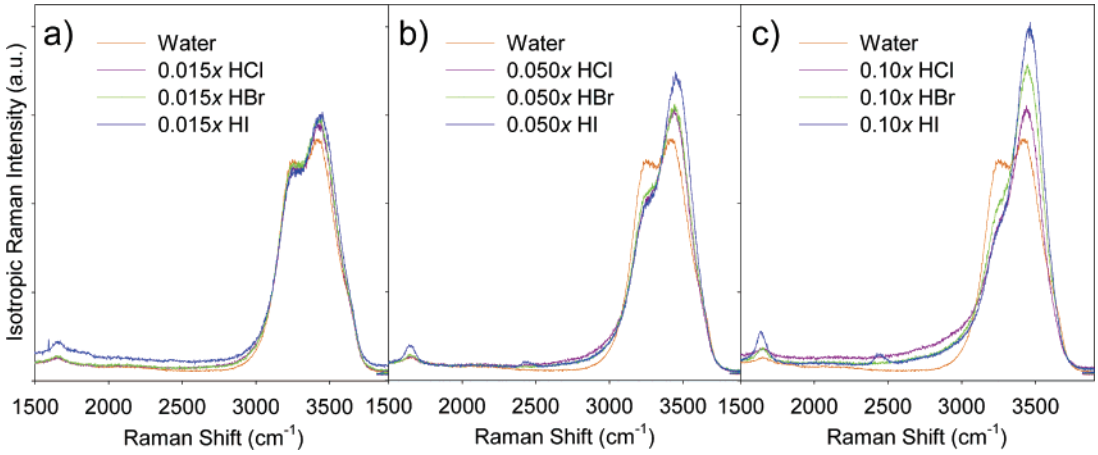

Figure 3. Isotropic Raman spectra of HCl, HBr, and HI aqueous solutions compared to that of neat water (a) 0.015*x*, (b) 0.050*x*, and (c) 0.10*x* series. (The slight baseline increase of the 0.015*x* HI spectrum is an artifact of the experiment.)

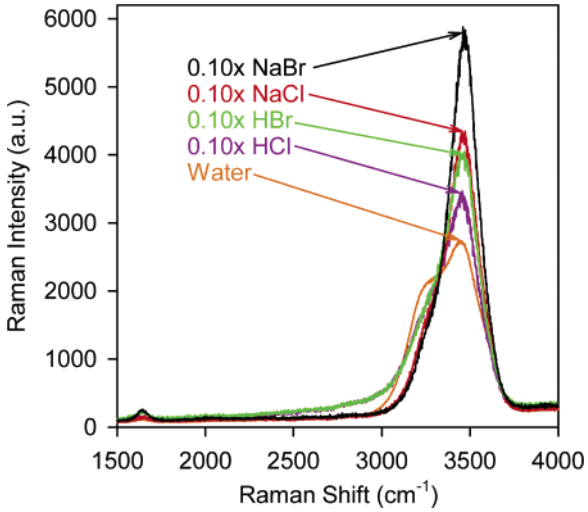

Figure 4. Unpolarized Raman spectra of 0.10*x* HCl, NaCl, HBr, and NaBr aqueous solutions compared to that of neat water.

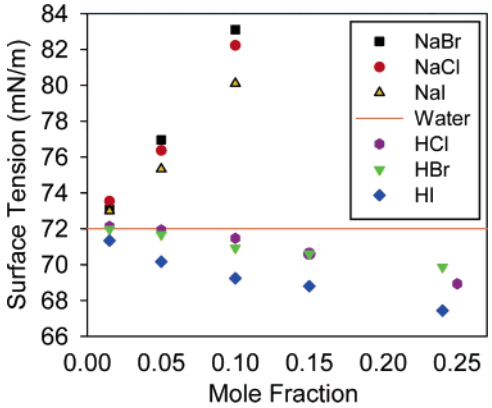

Figure 5. Surface tensions of acid and salt solutions (±1 standard deviation for all measurements are smaller than the size of the symbols).

The differences in the hydrogen-bonded stretching of the IR and Raman spectra of the acid solutions can be attributed to the different selection rules. For a mode to be Raman active, there must be a change in polarizability with the vibration. As acids with increasingly polarizable anions ($Cl^- < Br^- < I^-$) are added, the water molecules solvating these anions exhibit increased polarizability; thus, since Raman intensities arise from this condition, this effect is observed in the Raman spectra. For a mode to be IR active, the vibration must cause a change in the dipole moment. The polarity of the H_3O^+ and $H_5O_2^+$ ions is responsible for the strong proton continuum in the IR spectra.[41]

The broad band, between ~1500 and ~3200 cm^{-1}, present in the IR spectra (Figure 2) and to a lesser extent in the Raman spectra (Figure 3) of the acids arises from H_3O^+ and $H_5O_2^+$ groupings[37−40,42,43] due to the selection rules as stated above. The excess proton in the $H_5O_2^+$ groupings fluctuates very rapidly between the two water molecules due to the presence of a double-minimum or a broad flat potential well;[44] this potential well makes the hydrogen bonds extremely polarizable. Large hydrogen-bond polarizabilities result in various strong interactions (i.e., induced dipole interactions with ions and with dipole fields of the solute and solvent molecules and with each other) and distort the energy surfaces of the hydrogen bonds in $H_5O_2^+$.[37,38,42,43,45] The distortion of the energy surfaces is consistent with the protons within the hydrogen bonds having a continuous energy level distribution. Thus, a continuum in the IR and Raman spectra is observed.[37,38,45]

Much work has been done on the vibrational spectroscopy of H_3O^+ and $H_5O_2^+$ ions.[37−44,46,47] For example, Falk and Giguère observed strong, broad absorption bands in the infrared spectrum of aqueous acid solutions at about 1205, 1750, and 2900 cm^{-1} and attributed these to the hydronium ion.[41] Janoschek et al. were able to calculate the IR continua observed in aqueous solutions of strong acids and bases by taking into account distributions of electric field strengths and O−O distances. These calculations were able to reproduce the continua observed in aqueous solutions of HCl and H_2SO_4.[48] Clearly, the hydrogen-bonding environment of bulk water is strongly affected by the addition of hydrogen halides; yet, it is not clear what effect these ions have on the air−aqueous interface and thus is the focus of this work as discussed below.

Air−Aqueous Acid Interfaces. To examine the macroscopic view of the interface and gain further insight into the air−aqueous interface, surface tensions of the water and acid solutions were obtained and the results are shown in Figure 5. Upon the addition of acid, the surface tension decreases relative to that of water. HCl and HBr have approximately the same effect on the surface tension of water, whereas the effect of HI is much greater. In contrast, the addition of salts causes the surface tension of water to increase, consistent with previously reported surface tension data.[49]

Interpretation of the changes of surface tension with the addition of inorganic electrolytes is typically achieved via the

Gibbs adsorption equation, which predicts the net (positive or negative) ion excess in the interface.[50] An increase in surface tension with respect to neat water is explained by a net depletion of the surface layer by ions (both cations and anions). It is traditionally believed that inorganic aqueous salt solution surfaces are devoid of ions.[49−51] However, the studies presented here as well as molecular dynamics simulations[52−54] and other surface sensitive studies[13,55−59] have shown that ions are present in the air−aqueous interfacial region. These results are not a direct contradiction of the thermodynamic arguments based on the Gibbs adsorption equation, since these arguments do not account for the structure within the ion concentration profile (the surface enhancement and subsurface depletion). In the case of sodium salts (NaCl, NaBr, and NaI), the sodium ion tends to be repelled from the surface, while the halide ions have either a weak (Cl^-) or strong (Br^- and I^-) preference for the surface.[52,54] The combined effect of the two ions is an integrated net depletion of ions from the interfacial region.

Although the surface tension measurements give insight that the acids affect the surface water very differently than their corresponding sodium salts, it is not clear how the surface water structure will reorganize. To better understand the effect on the surface water structure, the air−aqueous interface of the acid solutions was investigated using VSFG spectroscopy. The resulting SSP-polarized VSFG spectra of the 0.015*x*, 0.050*x*, and 0.10*x* aqueous solutions of HCl, HBr, and HI are shown in Figure 6, panels a−c, respectively. The deviation in the VSFG signal in replicate runs was small; the HBr concentration series can be found in the Supporting Information as a representative set. The VSFG spectra were deconvoluted into the component peaks for interpretation (Table 2). The spectral fits of the 0.015*x* acids are shown in Figure 7 as an example. The component peaks are shown in red, and the calculated fits are green solid lines going through the majority of the data points. The corresponding fitting parameters for the acid solutions including relative phases (+ versus −) of the amplitude terms are shown in Table 2.

Recall the hydrogen-bonded stretching region at the air−aqueous interface of neat water is comprised of three component peaks: one at ∼3250 cm^{-1} arising from the DAA molecules in the interface with some contributions from SHB water molecules and the ∼3450 and ∼3550 cm^{-1} arising from the LSHB water molecules in the interface. In aqueous acid solutions, H_3O^+ (and $H_5O_2^+$) complexes existing in the interface give rise to an additional component peak centered at ∼3200 cm^{-1}. It is important to note that previous VSFG studies have shown that the corresponding salts (i.e., NaCl, NaBr, and NaI) do not give rise to an intensity increase in the 3200 cm^{-1} region, and therefore, it is highly unlikely that the halides play the dominant role in this intensity increase.[13] In general, the hydrogen-bonded stretching region in the VSFG spectra of the acids increases in intensity as the polarizability of the anion increases and as the acid concentration increases. In addition, as acid is added to neat water, the intensity of the free O−H peak substantially decreases, well resolved within our signal-to-noise.

The VSFG spectra show a significant intensity increase in the 3200 cm^{-1} region with the addition of acid as shown in Figure 6. An additional peak was required to fit the acid VSFG spectra in the 3200 cm^{-1} region separate from the 3250 cm^{-1} peak (the 3250 cm^{-1} peak follows the same trend as the free O−H peak, i.e., decreasing intensity with increasing acid concentration). The additional band at ∼3200 cm^{-1} in the VSFG spectra of the acids is assigned to a convolution of three factors: the presence of an interfacial potential resulting in a

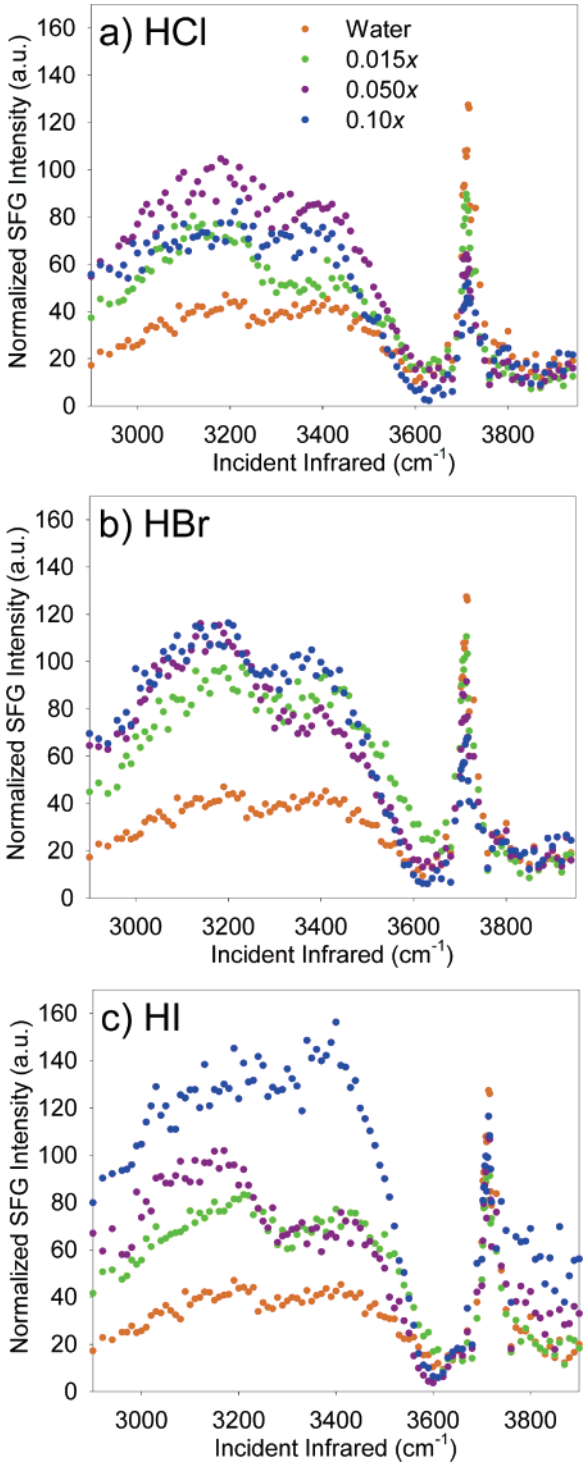

Figure 6. SSP-polarized VSFG spectra of acid solutions compared to that of neat water (a) HCl, (b) HBr, and (c) HI concentration series.

reorientation of the interfacial water molecules, probing more water molecules due to an increase in interfacial depth, and the presence of surface H_3O^+ and $H_5O_2^+$.

The first of three possible source of the VSFG intensity the 3200 cm^{-1} region is the presence of an interfacial potential. Recent MD simulations by Mucha et al.[54] support the proposed preferential orientation of the hydronium ions. This interfacial potential[60] results from the electrostatic field induced by the preferred orientation of the hydronium cations at the surface of the aqueous acid solutions.[49] The interfacial potential then serves to reorient the interfacial water molecules, resulting in an increase in the SSP VSFG intensity. The interfacial potential

TABLE 2: Parameters for VSFG Spectral Fits of 0.015*x*, 0.050*x*, and 0.10*x* Aqueous Solutions of HCl, HBr, and HI

VSFG											
nonresonant terms	peak position (cm^{-1})	phase	amplitude (A_v)	fwhm ($2\cdot\Gamma_v$)	area	nonresonant terms	peak position (cm^{-1})	phase	amplitude (A_v)	fwhm ($2\cdot\Gamma_v$)	area
neat water	3229	+	562.1	358.5	4410	**0.050*x* HBr**	3194	+	763.6	309.9	9650
	3443	+	524.1	242.5	6165		3239	+	449.1	358.5	2820
	3569	−	54.19	178.4	92		3434	+	636.5	242.5	9096
−2.864 + 1.1707*i*	3714	−	171.0	33.4	5413	−3.599 + 1.156*i*	3614	−	237.2	178.4	1749
	3748	−	241.5	125.2	2587		3715	−	137.0	33.4	3474
							3759	−	249.8	122.3	2822
0.015*x* HCl	3179	+	509.9	309.9	4172	**0.10*x* HBr**	3171	+	765.0	309.9	9630
	3235	+	480.7	358.5	3229		3250	+	397.1	358.5	2210
	3447	+	524.1	242.5	6163		3404	+	791.5	242.5	14080
−2.864 + 1.1708*i*	3569	−	69.19	178.4	150	−3.599 + 1.156*i*	3586	−	359.8	178.4	4047
	3715	−	145.0	33.4	3891		3715	−	117.0	33.4	2534
	3756	−	241.5	125.2	2576		3756	−	217.9	114.0	2328
0.050*x* HCl	3166	+	571.7	309.9	5370	**0.015*x* HI**	3200	+	574.5	351.7	4686
	3240	+	414.7	358.5	2405		3246	+	457.4	358.5	2929
	3419	+	657.9	246.0	9566		3444	+	682.4	242.5	10451
−3.102 + 2.103*i*	3589	−	153.2	178.4	733	−3.074 + 1.172*i*	3596	−	241.2	178.4	1815
	3715	−	125.0	33.4	2892		3715	−	140.0	33.4	3628
	3747	−	240.3	125.2	2561		3755	−	265.5	125.2	3145
0.10*x* HCl	3132	+	326.7	326.3	1627	**0.050*x* HI**	3164	+	578.1	351.7	4696
	3240	+	395.7	358.5	2190		3198	+	489.3	358.5	3319
	3420	+	623.1	248.4	8482		3442	+	835.2	242.5	14539
−3.656 + 4.440*i*	3589	−	203.3	178.4	1290	−3.856 + 1.870*i*	3550	−	491.2	178.4	7584
	3715	−	124.0	33.4	2846		3713	−	147.1	33.4	4008
	3742	−	198.7	169.8	1240		3756	−	360.5	129.7	5515
0.015*x* HBr	3200	+	565.7	309.9	5304	**0.10*x* HI**	3170	+	829.1	351.7	9681
	3257	+	497.4	358.5	3471		3286	+	424.1	358.5	2533
	3436	+	732.5	242.5	120449		3404	+	1035	242.5	22375
−2.864 + 1.171*i*	3610	−	195.2	178.4	1186	−4.473 + 1.882*i*	3560	−	558.2	178.4	9779
	3715	−	152.0	33.4	4276		3716	−	133.1	33.4	3275
	3756	−	242.2	125.2	2591		3755	−	486.4	134.2	9654

argument also supports the existence of a hydrated proton surface species since the enhancement of the 3200 cm^{-1} region is not observed in the halogen salt studies.[13,54,61] Shen and co-workers[24] and Ye et al.[62] have shown large enhancements in the 3200 cm^{-1} region arising from ordered water at charged quartz-water interfaces. Additionally, previous studies by Gragson et al.[63−65] have shown that the alignment of interfacial water molecules is observed as a large enhancement in the O−H stretching region of the VSFG spectra of ionic surfactants. These enhancements[24,62−65] are attributed to an alignment of the interfacial water molecules induced by the large electrostatic field present at these charged interfaces.

Eisenthal and co-workers[66,67] have explored the surface potential of aqueous insulating surfaces using second harmonic generation (SHG), discovering that the interface potential is linearly proportional to the SHG field. In addition, recent work by Shen and co-workers[25] provide additional evidence for the surface potential argument for the increased intensity in the 3200 cm^{-1} peak in the VSFG spectra of aqueous acid solutions. By exploiting the phase sensitivity of SFG and the 3-fold symmetry of a quartz crystal, these researchers were able to determine the orientation of water molecules with respect to the quartz surface.

A second possible contributing factor to the 3200 cm^{-1} intensity is due to an increase in the interfacial depth in the VSFG spectra of the acids. This explanation is consistent with previous studies on the aqueous halide salt solutions.[13,54] VSFG intensity (SSP polarization) is enhanced when probing larger numbers of hydrogen-bonded water molecules and/or an increased alignment of the symmetric stretch transition moment of water molecules along the surface normal. An interfacial depth increase (defined by an increase in noncentrosymmetry from the surface) will increase the number of water molecules providing an SFG signal. However, it is difficult to differentiate between the contributions of an increase in interfacial depth and changes in surface potential for the surface of halide acid solutions.

The third possible contribution is from H_3O^+ and $H_5O_2^+$ vibrational intensities. Existence of hydronium ions is a likely explanation for the intensity enhancement in the 3200 cm^{-1} region of the VSFG spectra that is consistent with recent experiments[54,68,69] and molecular dynamics simulations.[54,70] These simulations showed that the hydronium ion has an affinity for the surface of aqueous acid solutions with a preferred orientation with the hydrogens positioned toward the aqueous phase and oxygen toward the vapor phase. As shown in the work here, as the acid concentration is increased, more H_3O^+ (and $H_5O_2^+$) molecules are present in the interface and thus the intensity of the VSFG spectrum in the 3200 cm^{-1} region increases. However, it is unclear from the VSFG spectra if there is an enhancement of H_3O^+ and $H_5O_2^+$ relative to the bulk. Therefore, additional VSFG spectra were obtained to investigate the possible existence of a proton continuum as revealed in the Raman and IR spectra shown in Figures 2−4.

Lower frequency (2400−3200 cm^{-1}) VSFG spectra of neat water, 0.050*x* NaBr, and 0.050*x* HBr (Figure 8) were acquired to explore the enhanced intensity of the OH stretching region in the VSFG spectra of aqueous acid solutions and to provide further support for the existence of H_3O^+ and $H_5O_2^+$ in the interface. As shown in Figure 8, the VSFG spectra of aqueous NaBr solution has no enhanced intensity at frequencies in the range of 2400−3200 cm^{-1} as compared to that for neat water. However, the aqueous HBr solution VSFG spectra clearly show a significant intensity enhancement from 2700 to 3200 cm^{-1} when compared to both aqueous NaBr and neat water. (Spectral backgrounds on the same samples with the timing of the pulses

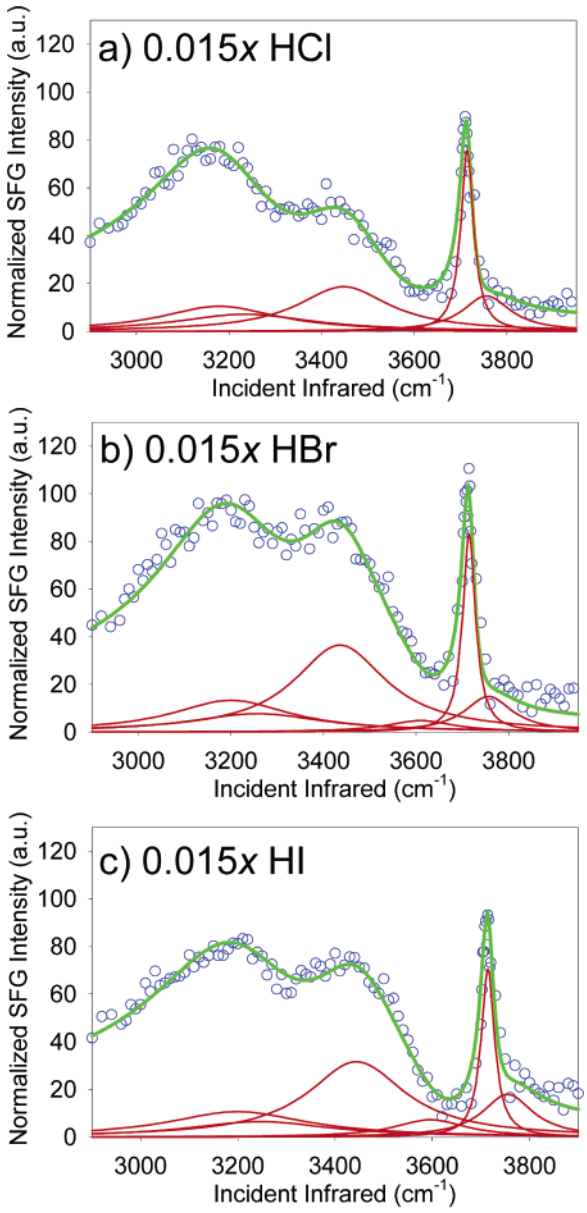

Figure 7. Spectral fits of the SSP-polarized VSFG spectra of 0.015*x* (a) HCl, (b) HBr, and (c) HI.

offset, as are typically done for control experiments, are shown as open squares.) The observed VSFG enhancement is consistent with the observed enhancements in IR (Figure 2) and Raman (Figure 3) spectra, that is, the proton continuum. This continuum clearly indicates that H_3O^+ (and/or $H_5O_2^+$) exists within the air−aqueous acid interface. Additionally, there is either a concentration gradient existing from the surface to the bulk, or subsurface structure (e.g., double layer), giving rise to a noncentrosymmetric region within the air−aqueous acid interface. This important result clearly lays to rest the question of hydrated protons in the interfacial region.

There have been several relevant studies that provide further insight into this remarkable result as discussed below. Saykally and co-workers[68] have clearly shown that iodide ions are enhanced at the air−water interface in aqueous HI as opposed to aqueous KI and NaI, inferring that hydronium is surface active and thereby allowing the iodide anions to be more surface active relative to the aqueous KI and NaI surfaces. Jungwirth and co-workers[54] postulate through MD simulation and VSFG data that hydronium exists in the interfacial region. Richmond and co-workers[69] also strongly suggest that hydronium resides in the

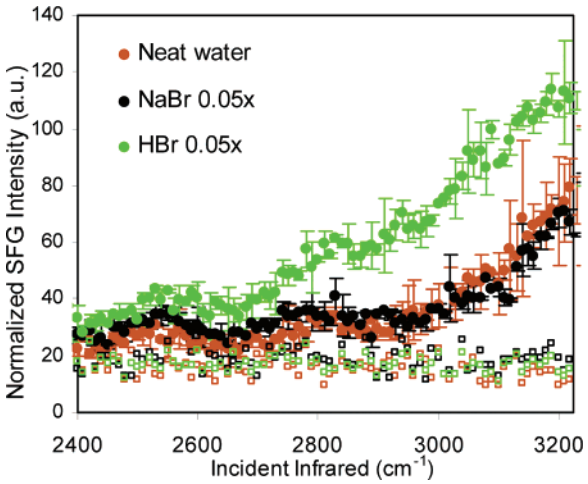

Figure 8. SSP-polarized VSFG spectra of 0.050*x* HBr (green solid circles) and 0.050*x* NaBr (black solid circles) compared to that of neat water (orange solid circles) showing the proton continuum arising from the 0.05 mole fraction HBr solution. The open squares are the corresponding HBr (green open squares), NaBr (black open squares), and neat water (orange open squares) background spectra (the visible and infrared input pulses were temporally misaligned at the sample). The open square data points show the actual background that contributes to the spectrum, confirming that the SFG intensities are real.

surface region of aqueous halogen acid solutions. With respect to surface H_3O^+, Lee and co-workers[46] observed the gas phase infrared spectra of the hydrated hydronium cluster ions $H_3O^+ \cdot (H_2O)_n$ ($n = 1-3$) from 3550 to 3800 cm^{-1}. Two features were visible for $H_5O_2^+$: a broad, featureless band at 3608.8 cm^{-1} and a higher frequency band centered at 3684.4 cm^{-1}. Graham and Roberts have also examined the infrared spectrum of the $HCl \cdot 6H_2O$ complex; vibrational modes centered at 1770 and 1275 cm^{-1} and the broad peak between 2500 and 3100 cm^{-1} were assigned to the ν_4, ν_2, and ν_3 modes of H_3O^+, respectively.[71] Scherer and co-workers[39] investigated the infrared spectra of HCl and HBr aqueous solutions and observed a continuous absorption from 1000 to 3400 cm^{-1} and three broad bands at 1760, 2900, and 3350 cm^{-1}, which are attributed to the hydrated proton.

In summary, it is clear that H_3O^+ and $H_5O_2^+$ exist at the air−aqueous acid interface and that the intensity of the VSFG spectra of aqueous acid solutions is likely a combination of surface H_3O^+ and $H_5O_2^+$ species. The presence of an interfacial potential resulting in a reorientation of the interfacial water molecules and the possibility of probing more water molecules due to an increase in interfacial depth likely contributes to the 3200 cm^{-1} VSFG enhancement but not to the lower frequency proton continuum. Identifying the degree of contribution from each component is not straightforward for the 3200 cm^{-1} region. Moreover, as is further discussed below, the proton continuum observed in Figure 8 provides strong evidence for the existence of hydrated protons within the air−aqueous acid interface.

To further evaluate the VSFG enhancement in the 3200 cm^{-1} region, the square root (SQRT) VSFG intensity of the 3200 cm^{-1} (added to the 3250 cm^{-1} peak intensity for normalization purposes) for the acid solutions relative to that of neat water are plotted in Figure 9a−c. Also shown in Figure 9a−c are the corresponding SQRT of the Raman times IR intensities for comparison. (The square roots of the intensities are plotted since these are directly proportional to the water molecule number density.) The SQRT of the Raman times IR intensities shows that there is a slight increase of the 3200 cm^{-1} peak as one goes from 0.015*x* to 0.10*x* for all of the acid solutions as

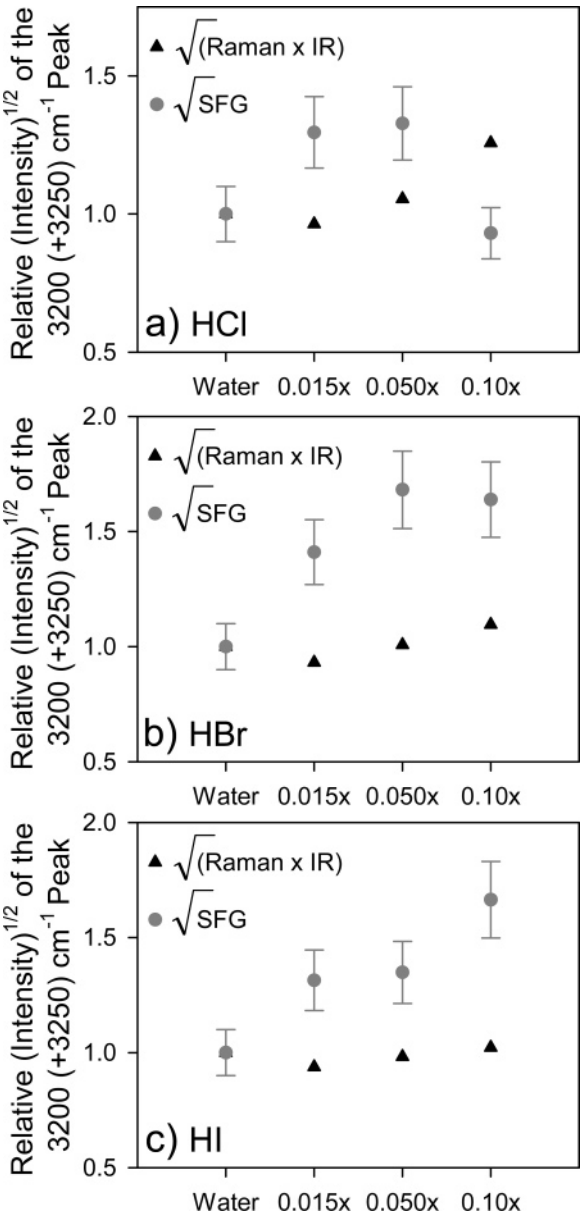

Figure 9. Plot of the relative (to water) square root intensities of the 3200 cm^{-1} peak (added to the 3250 cm^{-1} peak) for (a) HCl, (b) HBr, and (c) HI.

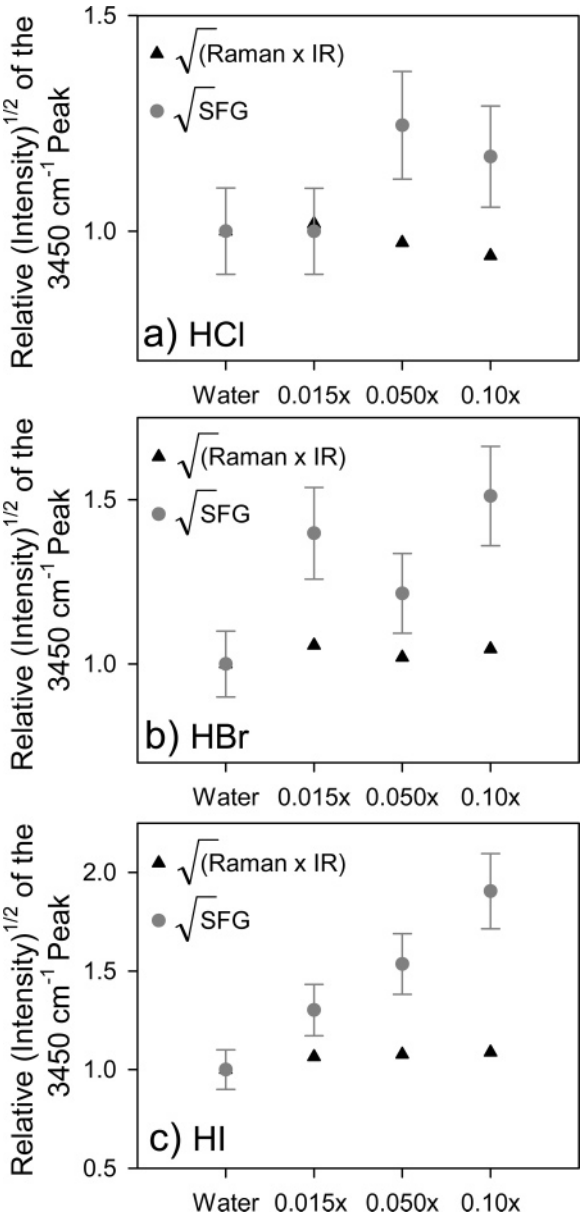

Figure 10. Plot of the relative (to water) square root intensities of the 3450 cm^{-1} peak for (a) HCl, (b) HBr, and (c) HI.

compared to water. The SQRT of the VSFG intensities of the 3200 cm^{-1} peak also shows an increase, but the enhancement is much greater. These data indicate that the observed changes are not due to a change in the transition moment strengths and provide support for, in addition to the existence of interfacial hydrated protons, an increasing interfacial depth and/or surface potential change (larger magnitude relative to neat water).

Consistent with the Raman contribution to the VSFG spectra, the acid VSFG spectra (Figure 6) also reveal an intensity enhancement in the LSHB 3450 cm^{-1} region. This increase in intensity (arising from 4-coordinate water molecules) increases according to the size and polarizability of the anion ($Cl^- < Br^- < I^-$) as well as with increasing concentration and is attributed to water molecules solvating the anions at the surface and thus disrupting the hydrogen-bonding network. This enhancement is consistent with previous studies on the sodium halide air−aqueous interfaces.[13] However, a change in surface potential would contribute to an increased VSFG intensity in the 3450 cm^{-1} region as well (as would additional anions brought to the surface by surface active hydronium[68]). Examination of Figure 10 shows that the enhancement in the VSFG intensity is much greater than that for the Raman times IR, indicating the enhancement in the LSHB 3450 cm^{-1} region may be due to ion solvation from an increase in number of anions in the interface, and possibly a change in surface potential, and an increase in interfacial depth as mentioned above.

It is also important to note that an examination of the infrared and Raman spectral fits relative to the VSFG fits as shown in Figures 9 and 10 permit the exclusion of an increase in the infrared and Raman transition moment strengths being the cause of the additional VSFG enhancement in the hydrogen-bonded stretching region. An electric double layer formation can also be excluded based on recent molecular dynamics simulations on aqueous solutions of HCl, HBr, and HI.[54] For HCl, both the hydronium cations and the chloride anions were predicted to be present at the air−aqueous interface, with both showing a slight surface ion enhancement. The density profiles for HBr and HI showed a similar picture, except that bromine and iodine were more surface enhanced than chloride or hydronium. These simulations revealed that the separation of cations and anions at the aqueous-air interface is not extensive and the formation

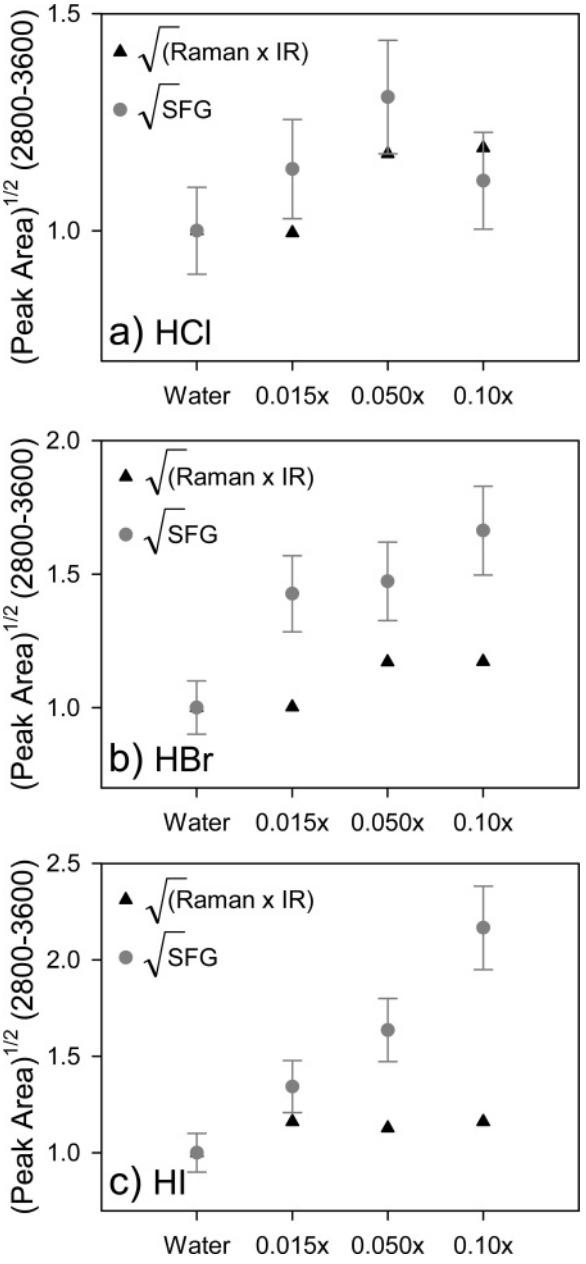

Figure 11. Plot of the relative square root areas of the 3200, 3250, 3450, and 3550 cm^{-1} (approximate, positions varied) peaks in the O−H stretch region for Raman × infrared (Raman area multiplied by ATR-FTIR area) and the SFG for the (a) HCl, (b) HBr, and (c) HI acid concentrations. Areas were normalized to neat water. Error bars are estimated to be approximately 10%, based on experimental values.

of an electric double layer at the surface of aqueous acid solutions is unlikely.

To further explore the differences in the air−aqueous interface arising from the addition of hydronium, chloride, bromide and iodide ions, plots of the SQRT VSFG intensities were assessed to better understand the general trends as acid concentration was increased as shown in Figures 9−11. Overall, these figures confirm the observed spectral trends, but also show some interesting anomalies. The general trend is that as the acid concentration and/or the size and polarizability of the anion (Cl^- < Br^- < I^-) are increased, the relative SQRT intensities of the 3200 cm^{-1} peak (added to the 3250 cm^{-1} peak) (Figure 9) and the 3450 cm^{-1} peak (Figure 10) and the additive peak areas of the component peaks (Figure 11) increase. However, intensity anomalies occur at the highest concentration of HCl. At 0.10*x*

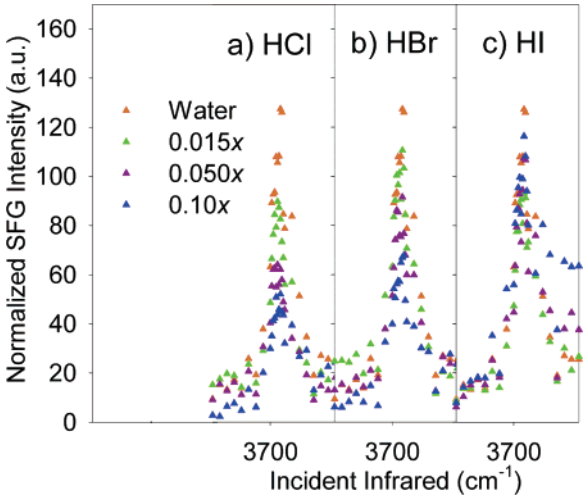

Figure 12. Free OH region of the VSFG spectra of (a) HCl, (b) HBr, and (c) HI.

HCl, the SQRT VSFG intensity of the 3200 cm^{-1} peak decreases to an intensity close to that for neat water (Figure 9). This deviation for the 0.10*x* HCl is also observed in the additive peak areas (Figure 11). Another interesting anomaly occurs in the 3450 cm^{-1} peak at 0.050*x* (Figure 10). For HCl and HI, the SQRT relative intensities for 0.050*x* are greater than that for 0.015*x*, but the SQRT intensity for 0.015*x* HBr is increased relative to 0.050*x*. It is not completely clear why the anomalies exist, yet this indicates a difference of interfacial structure with increasing concentration.

The VSFG spectra of the acid solutions also reveal a decrease in the 3700 cm^{-1} peak (free O−H stretch) intensity relative to neat water as shown in Figures 12 and 13. Although clearly resolved in our spectra due to excellent signal-to-noise and confirmed through fits (Figure 13) and is also shown in work completed by Shultz and co-workers,[28,72] others have not observed this to the same extent.[69] Upon the addition of the halogen acids, the surface water structure undergoes a structural reorganization that reduces the number of O−H bonds projecting into the air. As the acid concentration is increased from 0.015*x* to 0.050*x* to 0.10*x*, the free O−H peak intensity continues to decrease, indicating that the increasing presence of H_3O^+ (and $H_5O_2^+$) ions in the interface plays a significant role in the surface reorganization. In Figure 13, the SQRT of the 3700 cm^{-1} peak is shown to decrease by ∼25% from that of neat water to that of 0.10*x*, indicating a reduction of the free O−H by ∼25%. Assuming that the transition moment strength has not changed relative to neat water, and that at the neat water surface ∼20% of the water molecules have a free O−H extending into the air−phase,[26] the free O−H now makes up only ∼15% of the surface.

No enhancement in the free O−H stretching region of the SPS-polarized VSFG spectra was observed, confirming the number of free hydroxyl groups is decreased rather than oriented differently with the addition of acid. Reorientation of the free O−H bonds to hydrogen bond with the oxygens of the hydronium ions is also not a rational explanation since there is a hydrophobic region on the lone-pair side of the oxygen in the hydronium ion.[70] However, the observed decrease in the free O−H peak intensity of the VSFG spectra is consistent with molecular dynamics simulations.[54] In the MD study,[54] the surface density (number per unit area) of free O−H bonds was calculated for the aqueous solutions of NaCl, NaOH, HCl, and HBr and compared to that for neat water. In the sodium salt and base solutions, the density of free O−H bonds was about

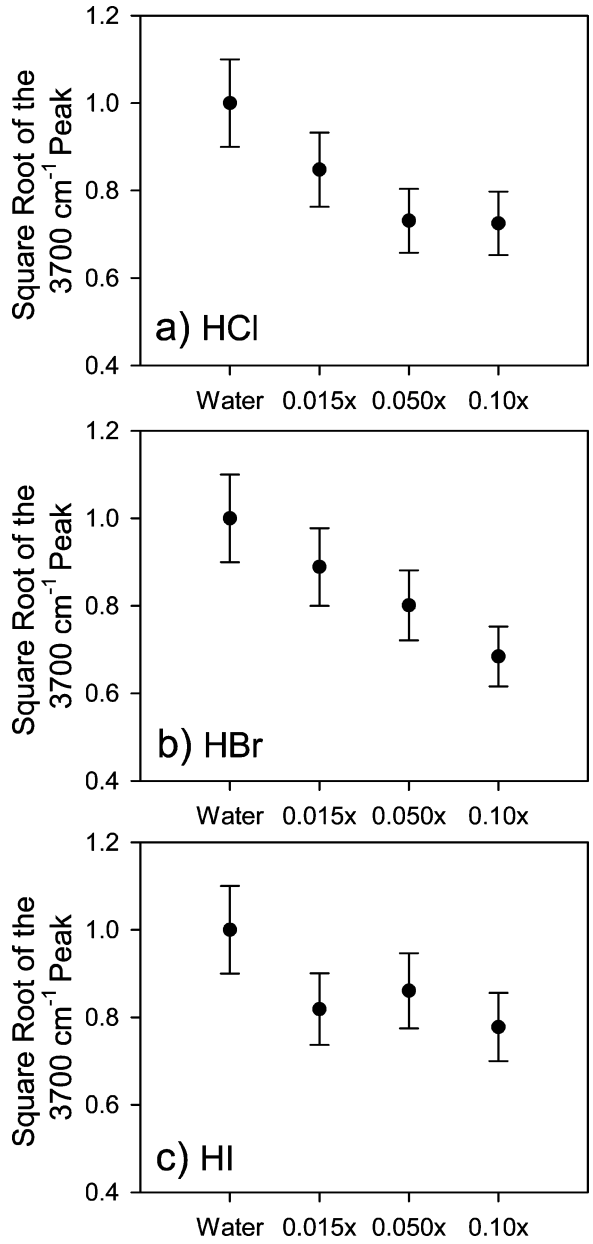

Figure 13. Plot of the relative (to water) square root intensities of the 3700 cm^{-1} peak for (a) HCl, (b) HBr, and (c) HI.

the same as neat water, whereas in HCl and HBr, there was a significant reduction in the surface density. The lack of changes in the surface orientation distribution was also confirmed through angular distribution calculations.[54]

In light of the recent sodium halide studies of surface water structure[13,55,57,60,73] and the studies presented here, replacement of the sodium cation with a hydrated proton clearly causes a significant perturbation to the air−aqueous interface. Changes in the surface potential combined with accessibility of hydrated protons and halides to the surface region provide an evolving picture of the surface of atmospheric aerosols containing these species. The pH of aqueous atmospheric aerosols can vary significantly, from slightly basic to completely neutral to strongly acidic.[74] In the studies presented here, we have elucidated the surface structure of aqueous acid solution with calculated pHs of 0.09 to −0.72. Clearly, adsorption properties and potential reactions at the surface and in the bulk of atmospheric aerosols may be impacted by the existence of the hydrated protons and halides in the interface.

IV. Conclusions

The air−liquid interface of aqueous hydrogen−halide (i.e., strong acid) solutions was investigated using vibrational sum frequency generation spectroscopy complemented by surface tension measurements. The effect of these ions on the bulk water structure was also studied using IR and Raman spectroscopies. Within the bulk liquid environment for the aqueous hydrochloric, hydrobromic, and hydriodic acid solutions, the hydrogen-bonding network of water becomes increasingly disrupted by the solvation shells of the anion as the size, polarizability, and concentration of the anions is increased. Enhanced intensity was observed in the water O−H stretching modes at the air−liquid interface of the 0.015*x* hydrochloric, hydrobromic, and hydriodic acid solutions; the intensity was further enhanced as the acid concentration was increased to 0.050*x* and 0.10*x*. Comparison of the bulk and interfacial spectra of the HCl, HBr, and HI aqueous solutions indicates several contributions: the presence of H_3O^+ (and $H_5O_2^+$), bromide, and iodide ions at the air−liquid interface, the presence of an electrostatic field which creates a surface potential of greater magnitude than that from neat water, and thus aligning interfacial water molecules, and an increase in interfacial depth relative to that of neat water. The surface potential changes arise from the interfacial population of the ions, inclusive of the hydrated protons and halides. And most notable, is the enhanced VSFG intensities below 3000 cm^{-1}, clearly indicating that hydrated protons, H_3O^+ and $H_5O_2^+$, are present in the air−liquid interfacial region between air and aqueous halogen acids.

Acknowledgment. We acknowledge NSF for funding this project through the NSF-Atmospheric Sciences award #ATM-0413893. We also acknowledge funding from Research Corporation (Research Innovation Award) for initiating the aqueous acid project. We also acknowledge contributions from Lisa (Nikki) Fox through the NSF REU program.

Supporting Information Available: Anisotropic and higher resolution unpolarized Raman spectra and the IR spectrum of 6.1 M NaBr are included. VSFG spectral alternative fits are shown. VSFG spectra of the HBr acid series with error bars are also shown. Additionally, conversions between mole fraction and molarity of the aqueous solutions are included. This material is available free of charge via the Internet at http://pubs.acs.org.

References and Notes

(1) Finlayson-Pitts, B. J. *Chem. Rev.* **2003**, *103*, 4801−4822.
(2) De Haan, D. O.; Brauers, T.; Oum, K.; Stutz, J.; Nordmeyer, T.; Finlayson-Pitts, B. J. *Int. Rev. Phys. Chem.* **1999**, *18*, 343−385.
(3) Knipping, E. M.; Lakin, M. J.; Foster, K. L.; Jungwirth, P.; Tobias, D. J.; Gerber, R. B.; Dabdub, D.; Finlayson-Pitts, B. J. *Science* **2000**, *288*, 301−306.
(4) Bloembergen, N.; Pershan, P. S. *Phys. Rev.* **1962**, *128*, 606−622.
(5) Hirose, C.; Akamatsu, N.; Domen, K. *Appl. Spectrosc.* **1992**, *46*, 1051−1072.
(6) Miranda, P. B.; Shen, Y. R. *J. Phys. Chem. B* **1999**, *103*, 3292−3307.
(7) Morita, A.; Hynes, J. T. *Chem. Phys.* **2000**, *258*, 371−390.
(8) Shen, Y. R. *The Principles of Nonlinear Optics*, 1st ed.; John Wiley & Sons: New York, 1984.
(9) Bain, C. D. *J. Chem. Soc., Faraday Trans.* **1995**, *91*, 1281−1296.
(10) Moad, A. J.; Simpson, G. J. *J. Phys. Chem. B* **2004**, *108*, 3548−3562.
(11) Lambert, A. G.; Davies, P. B.; Neivandt, D. J. *Appl. Spectrosc. Rev.* **2005**, *40*, 103−145.
(12) Zhang, D.; Gutow, J.; Eisenthal, K. B. *J. Phys. Chem.* **1994**, *98*, 13729−13734.
(13) Liu, D.; Ma, G.; Levering, L. M.; Allen, H. C. *J. Phys. Chem. B* **2004**, *108*, 2252−2260.

(14) McCreery, R. L. *Raman Spectroscopy for Chemical Analysis*; John Wiley & Sons: New York, 2000.
(15) Benjamin, I. *Phys. Rev. Lett.* **1994**, *73*, 2083−2086.
(16) Berne, B. J.; Pecora, R. *Dynamic Light Scattering: With Applications to Chemistry, Biology and Physics*; Dover Publications, Inc.: New York, 2000.
(17) Eaves, J. D.; Loparo, J. J.; Fecko, C. J.; Roberts, S. T.; Tokmakoff, A.; Geissler, P. L. *Proc. Natl. Acad. Sci.* **2005**, *102*, 13019−13022.
(18) Smith, J. D.; Cappa, C. D.; Wilson, K. R.; Cohen, R. C.; Geissler, P. L.; Saykally, R. J. *Proc. Natl. Acad. Sci.* **2005**, *102*, 14171−14174.
(19) Buch, V.; Devlin, J. P. *J. Chem. Phys.* **1999**, *110*, 3437−3443.
(20) Andersson, P.; Steinbach, C.; Buck, U. *Eur. Phys. J. D.* **2003**, *24*, 53−56.
(21) Corcelli, S. A.; Skinner, J. L. *J. Phys. Chem. A* **2005**, *109*, 6154−6165.
(22) Steinbach, C.; Andersson, P.; Kazimirski, J. K.; Buck, U.; Buch, V.; Beu, T. A. *J. Phys. Chem. A* **2004**, *108*, 6165−6174.
(23) Devlin, J. P.; Sadlej, J.; Buch, V. *J. Phys. Chem. A* **2001**, *105*, 974−983.
(24) Ostroverkhov, V.; Waychunas, G. A.; Shen, Y. R. *Chem. Phys. Lett.* **2004**, *386*, 144−148.
(25) Ostroverkhov, V.; Waychunas, G. A.; Shen, Y. R. *Phys. Rev. Lett.* **2005**, *94*, 46102.
(26) Du, Q.; Superfine, R.; Freysz, E.; Shen, Y. R. *Phys. Rev. Lett.* **1993**, *70*, 2313−2316.
(27) Radüge, C.; Pflumio, V.; Shen, Y. R. *Chem. Phys. Lett.* **1997**, *274*, 140−144.
(28) Gopalakrishnan, S.; Liu, D.; Allen, H. C.; Kuo, M.; Shultz, M. J. *Chem. Rev.* **2006**, *106*, 1155−1175.
(29) Walker, D. S.; Hore, D. K.; Richmond, G. L. *J. Phys. Chem. B* **2006**, *110*, 20451−20459.
(30) Allen, H. C.; Raymond, E. A.; Richmond, G. L. *J. Phys. Chem. A* **2001**, *105*, 1649−1655.
(31) Schnitzer, C.; Baldelli, S.; Campbell, D. J.; Shultz, M. J. *J. Phys. Chem. A* **1999**, *103*, 6383−6386.
(32) McCoy, A. B. Ohio State University, Columbus, OH. Private communication, 2006.
(33) Buck, U.; Ettischer, I.; Melzer, M.; Buch, V.; Sadlej, J. *Phys. Rev. Lett.* **1998**, *80*, 2578−2581.
(34) Shin, J.-W.; Hammer, N. I.; Diken, E. G.; Johnson, M. A.; Walters, R. S.; Jaeger, T. D.; Duncan, M. A.; Christie, R. A.; Jordan, K. D. *Science* **2004**, *304*, 1137−1141.
(35) Buch, V.; Devlin, J. P. *J. Chem. Phys.* **1991**, *94*, 4091−4092.
(36) Rowland, B.; Fisher, M.; Devlin, J. P. *J. Chem. Phys.* **1991**, *95*, 2485−2487.
(37) Zundel, G. Easily Polarizable Hydrogen Bonds-Their Interactions With the Environment-IR Continuum and Anomalous Large Proton Conductivity. In *The Hydrogen Bond, Recent developments in theory and experiments*; Schuster, P., Zundel, G., Sandorfy, C., Eds.; North-Holland Publishing Company: Amsterdam, 1976; Vol. 2, pp 683−766.
(38) Roberts, N. K.; Zundel, G. *J. Phys. Chem.* **1980**, *84*, 3655−3660.
(39) Kim, J.; Schmitt, U. W.; Gruetzmacher, J. A.; Voth, G. A.; Scherer, N. E. *J. Chem. Phys.* **2002**, *116*, 737−746.
(40) Asmis, K. R.; Pivonka, N. L.; Santambrogio, G.; Brümmer, M.; Kaposta, C.; Neumark, D. M.; Wöste, L. *Science* **2003**, *299*, 1375−1377.
(41) Falk, M.; Giguère, P. A. *Can. J. Chem.* **1957**, *35*, 1195−1204.
(42) McCoy, A. B.; Huang, X.; Carter, S.; Landeweer, M. Y.; Bowman, J. M. *J. Chem. Phys.* **2005**, *122*, 061101−1.-061101−4.
(43) Diken, E. G.; Headrick, J. M.; Roscioli, J. R.; Bopp, J. C.; Johnson, M. A.; McCoy, A. B. *J. Phys. Chem. A Lett.* **2005**, *109*, 1487−1490.
(44) Headrick, J. M.; Diken, E. G.; Walters, R. S.; Hammer, N. I.; Christie, R. A.; Cui, J.; Myshakin, E. M.; Duncan, M. A.; Johnson, M. A.; Jordan, K. D. *Science* **2005**, *308*, 1765−1769.
(45) Janoschek, R.; Weidemann, E. G.; Pfeiffer, H.; Zundel, G. *J. Am. Chem. Soc.* **1972**, *94*, 2387−2396.
(46) Yeh, L. I.; Okumura, M.; Myers, J. D.; Price, J. M.; Lee, Y. T. *J. Chem. Phys.* **1989**, *91*, 7319−7330.
(47) Hammer, N. I.; Diken, E. G.; Roscioli, J. R.; Johnson, M. A.; Myshakin, E. M.; Jordan, K. D.; McCoy, A. B.; Huang, X.; Bowman, J. M.; Carter, S. *J. Chem. Phys.* **2005**, *122*, 244301−244309.
(48) Janoschek, R.; Hayd, A.; Weidemann, E. G.; Leuchs, M.; Zundel, G. *J. Chem. Soc., Faraday Trans. 2* **1978**, *74*, 1238−1245.
(49) Randles, J. E. B. *Phys. Chem. Liq.* **1977**, *7*, 107−179.
(50) Adam, N. K. *The Physics and Chemistry of Surfaces*; Oxford University Press: London, 1941.
(51) Onsager, L.; Samaras, N. N. T. *J. Chem. Phys.* **1934**, *2*, 528−536.
(52) Jungwirth, P.; Tobias, D. J. *J. Phys. Chem. B* **2002**, *106*, 6361−6373.
(53) Dang, L. X.; Chang, T.-M. *J. Phys. Chem. B* **2002**, *106*, 235−238.
(54) Mucha, M.; Frigato, T.; Levering, L. M.; Allen, H. C.; Tobias, D. J.; Dang, L. X.; Jungwirth, P. *J. Phys. Chem. B* **2005**, *109*, 7617−7623.
(55) Ghosal, S.; Hemminger, J. C.; Bluhm, H.; Mun, B. S.; Hebenstreit, E. L. D.; Ketteler, G.; Ogletree, D. F.; Requejo, F. G.; Salmeron, M. *Science* **2005**, *307*, 563−566.
(56) Ghosal, S.; Shbeeb, A.; Hemminger, J. C. *Geophys. Res. Lett.* **2000**, *27*, 1879−1882.
(57) Petersen, P. B.; Johnson, J. C.; Knutsen, K. P.; Saykally, R. J. *Chem. Phys. Lett.* **2004**, *397*, 46−50.
(58) Baldelli, S.; Schnitzer, C.; Shultz, M. J. *Chem. Phys. Lett.* **1999**, *302*, 157−163.
(59) Petersen, P. B.; Saykally, R. J. *J. Phys. Chem. B* **2006**, *110*, 14060−14073.
(60) Petersen, M. K.; Saykally, R. J. *Annu. Rev. Phys. Chem.* **2006**, *57*, 333−364.
(61) Shultz, M. J.; Schnitzer, C.; Simonelli, D.; Baldelli, S. *Int. Rev. Phys. Chem.* **2000**, *19*, 123−153.
(62) Ye, S.; Nihonyanagi, S.; Uosaki, K. *Chem. Lett.* **2000**, 734−735.
(63) Gragson, D. E.; McCarty, B. M.; Richmond, G. L. *J. Am. Chem. Soc.* **1997**, *119*, 6144−6152.
(64) Gragson, D. E.; Richmond, G. L. *J. Am. Chem. Soc.* **1998**, *120*, 366−375.
(65) Gragson, D. E.; Richmond, G. L. *J. Phys. Chem. B* **1998**, *102*, 3847−3861.
(66) Eisenthal, K. B. *Acc. Chem. Res.* **1993**, *26*, 636−643.
(67) Zhao, X.; Ong, S.; Eisenthal, K. B. *Chem. Phys. Lett.* **1993**, *202*, 513−520.
(68) Petersen, M. K.; Saykally, R. J. *J. Phys. Chem. B* **2005**, *109*, 7976−7980.
(69) Tarbuck, T. L.; Ota, S. T.; Richmond, G. L. *J. Am. Chem. Soc.* **2006**, *128*, 14519−14527.
(70) Petersen, M. K.; Iyengar, S. S.; Day, T. J. F.; Voth, G. A. *J. Phys. Chem. B* **2004**, *108*, 14804−14806.
(71) Graham, J. D.; Roberts, J. T. *Chemom. Intell. Lab. Syst.* **1997**, *37*, 139−148.
(72) Schnitzer, C.; Baldelli, S.; Shultz, M. J. *J. Phys. Chem. B* **2000**, *104*, 585−590.
(73) Raymond, E. A.; Richmond, G. L. *J. Phys. Chem. B* **2004**, *108*, 5051−5059.
(74) Keene, W. C.; Sander, R.; Pszenny, A. A. P.; Vogt, R.; Crutzen, P. J.; Galloway, J. N. *J. Aerosol Sci.* **1998**, *29*, 339−356.